Composites: Part A 102 (2017) 96–107

Contents lists available at ScienceDirect

Composites: Part A

journal homepage: www.elsevier.com/locate/compositesa

Simulation-driven mold compensation strategy for composites: Experimental validation on a doubly-curved part

B. Wucher [a,*], Ph. Martiny [b], F. Lani [c], T. Pardoen [d], C. Bailly [e], D. Dumas [a]

[a] Methods for Structural Applications and Processes, Cenaero, Rue des Frères Wright 29, B-6041 Gosselies, Belgium
[b] e-Xstream Engineering, MSC Software, Rue Emile Francqui 9, B-1435 Mont-Saint-Guibert, Belgium
[c] Any-Shape, Rue de la Digue 37, B-4400 Flémalle, Belgium
[d] Institute of Mechanics, Materials and Civil Engineering, Université catholique de Louvain, Place Sainte Barbe 2, B-1348 Louvain-la-Neuve, Belgium
[e] Institute of Condensed Matter and Nanosciences, Université catholique de Louvain, Croix du Sud 1, B-1348 Louvain-la-Neuve, Belgium

ARTICLE INFO

Article history:
Received 17 January 2017
Received in revised form 17 July 2017
Accepted 29 July 2017
Available online 1 August 2017

Keywords:
Mold compensation
C. Finite element analysis (FEA)
E. Cure
E. Tooling

ABSTRACT

Thermoset-based composites exhibit irreversible distortions during manufacturing, which are detrimental to the assembly and then to the mechanical integrity. The optimal mold geometry can be determined by numerical simulation such that the produced composite component matches the target design. A simple mold compensation methodology as well as an all-around experimental validation are proposed for a doubly-curved part made of a carbon fiber reinforced composite. Non-compensated and compensated parts are processed in order to quantify the gain obtained by the compensation procedure and to validate the method. The spring-in is reduced by more than 90% and the overall distortions are reduced by about 70%.

1. Introduction

Thermoset-based continuous fiber reinforced composites exhibit irreversible distortions during manufacturing. These distortions are caused by a variety of phenomena, including thermal and chemical strains, tool-part interaction, or anisotropy of the composite [1]. Assembling out-of-tolerance structures is problematic and requires the application of mechanical loads, leading either to failure or to internal stresses detrimental to the in-service life of the material [2]. Although cure-induced distortions constitute a major topic of attention in the composite literature, only few attempts have been made to address in a systematic way the reduction or, better, the suppression of the problem. Two main approaches can be followed.

A first option is to improve the manufacturing process. Teoh and Hsiao [3] observed a spring-in reduction of L-shaped parts through a multistage curing schedule via the VARTM process. Hsiao and Gangireddy [4] proposed to include carbon nanofibers in a polyester resin in order to reduce the anisotropy in the thermal expansion of the material and, hence, to limit the spring-in. Both of these methods drastically increase the complexity of the manufacturing process. Jain et al. [5] optimized experimentally the spring-in of a thermoplastic C-shaped aileron rib by changing the cure temperature. These three examples rely on time-consuming experimental investigations, with trial-and-error sequences. Brauner [6] suggested the application of a non-uniform curing cycle to an RTM press. In this scenario, the temperature of each zone of the press would be predicted by simulation in order to decrease the overall distortions of a composite part. The author showed numerically that a thermal gradient can decrease the warpage of a wing panel, but the applicability of a truly optimized approach was not demonstrated. In particular, it was acknowledged that very high temperature gradients are required which creates a series of other unsolved problems.

The second option consists in using numerical simulations to guide the selection of the optimal geometry of the mold so that the cured part is as close as possible to the target geometry. This approach is called "mold compensation" and is the subject of the present study. Dong [7] developed a simplified curing model, created designs of experiments for several basic composite structures with only a few parameters and obtained a regression-based spring-in reduction method. Dong [8] studied the effect of the curing process on a parametrized stiffener structure, but without including the model in an optimization loop. Zhu and Geubelle [9] used an optimizer to alter the mold shape for L-shaped parts. Kappel et al. [10] took advantage of the morphing function of the software CATIA in order to compensate the warpage of flat plates made of unidirectional carbon/epoxy prepregs. Single-curvature warpage predictions for any possible stacking sequence were

* Corresponding author.
E-mail address: benoit.wucher@cenaero.be (B. Wucher).

http://dx.doi.org/10.1016/j.compositesa.2017.07.029
1359-835X/

obtained from interpolated measurements of a series of manufactured specimens of different lengths and thicknesses. The fact that the model is calibrated on experimental data diminishes the applicability of the method to other geometries and materials. Moreover, the author did not check, numerically or experimentally, that the compensated mold shape indeed produces flat panels after cure. Jung et al. [11] performed the same study for hybrid glass/-carbon composite beams and achieved satisfactory compensation. Kappel et al. [2] compensated a straight C—profile, once again relying on experimental measurements of the spring-in affecting a significant number of L-shaped brackets. All the aforementioned studies remain within the single-curvature range where the distortions can be, in a first approximation, compensated by a simple inversion. Fernlund et al. [12] developed process modeling capabilities and applied them to tool compensation involving several distortion modes of curved L-angles [13]. The compensation strategy was solely based on analytical considerations specific to this geometry. This case study has later been included in a risk assessment framework which quantified the probability that the manufactured parts are out of tolerances [14]. Hörberg et al. [15] aimed to compensate a highly-integrated 9 m long stiffened upper wing cover. To this end, they simulated and compensated a 1 m long panel. No indication was provided regarding the compensation methodology and the distortions of the full-scale wing were not measured.

Wucher et al. [16] proposed two CAD-centric optimization methods which allowed a reduction of the residual distance between the cured geometry and the target design. While the generic aspect of these methods makes them applicable to a wide range of complex geometries, the high computational cost motivated the development of a simpler methodology which is described in the present paper. Moreover, the literature deeply lacks experimental evidence that compensation methods actually lead to composite parts with drastically reduced distortions in the case of non-trivial geometries. An experimental validation of the compensation procedure on a doubly-curved composite part is the main objective of this paper, which is organized as follows. Section 2 presents a simple simulation-driven compensation methodology based on iterative alterations of the Finite Element (FE) mesh of the target geometry. Section 3 briefly describes the selected geometry and materials for the experimental validation. Section 4 explains the experimental procedure used to manufacture the composite parts. Section 5 provides details about the numerical model which is used, including the material properties. Finally, Section 6 presents an in-depth analysis and discussion of the results.

2. Numerical compensation procedure

The numerical compensation procedure, called the “mirror method”, is based on the simplifying assumption that cure-induced distortions can be considered in a first approximation as geometrically linear. Under this hypothesis, the compensated geometry should thus be close to the inverted cured geometry with respect to the target geometry. An iterative alteration of the mesh is performed based on the procedure schematically described in Fig. 1. A composite flat plate is drawn as a 1D line in order to simplify the representation. At iteration 0, the distortions of the target geometry are predicted by the numerical model described in Section 5. The tool geometry at iteration 1 is the inversion of this cured geometry, after a best-fit alignment. The cure-induced distortions of the part based on this tool geometry are then predicted. Logically, this cured geometry should be closer to the target geometry than the cured geometry at iteration 0. What is missing for the cured geometry to be equal to the target geometry is added to the tool geometry, resulting in the tool geometry of iteration 2. This

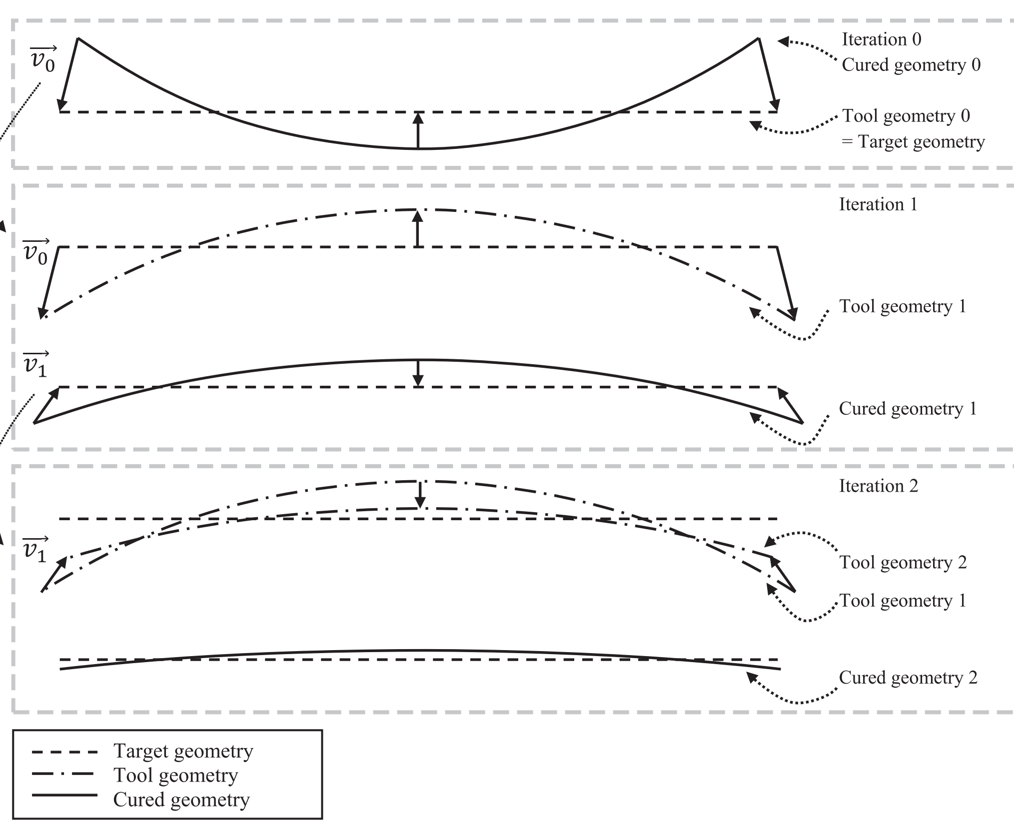

Fig. 1. Schematic description of the mirror mold compensation method.

process continues until the cured geometry converges towards the target geometry. If M_0^i and M_C^i are the meshes of the composite part before and after the curing simulation at iteration i, respectively (M_0^i can be assimilated to the tool geometry at iteration i), the corrected mesh for the next iteration is defined as

$$M_0^{i+1} = M_0^i + \left(M_0^0 - M_C^i\right), \tag{1}$$

where M_0^0 is the mesh of the target geometry. Although it does not appear in the schematics of Fig. 1, the correction of the geometry is actually performed based on the meshes, and Eq. (1) is applied node by node. The material orientations (directions of orthotropy) for each element are updated for the corrected mesh based on vector projections from the mesh of the target geometry to the corrected mesh. This approach may seem like basic common sense and the question must be raised whether or not the development of more sophisticated CAD-based methods, such as in [16], brings any advantage.

This question is addressed in Fig. 2. It presents the convergence history of the residual distance D_{min} when applying the mirror method to different types of geometries. The parameter D_{min} is a node-to-node residual distance after a best-fit alignment between the cured geometry and the target geometry as described by Wucher et al. [16]. The purpose of mold compensation is to bring D_{min} down to zero. The method is applied to a flat plate with an asymmetrical layup, to a generic doubly-stiffened panel, to a 1 m long curved Z-shaped panel with stiffeners and multiple drop-offs, to simple straight Z-shaped brackets, and to a doubly-curved C-spar. Fig. 2 shows that the mirror method converges very fast for geometries involving distortions dominated by spring-in, while it stagnates or diverges for warpage-dominated structures. This is explained by the fact that this compensation method assumes a more or less linear behavior of the cure-induced distortions which is not always correct. This is particularly striking in the case of the asymmetric flat plate in Fig. 2: the flat plate distorts into a saddle shape, due to the competing thermal and chemical strains of its lower and upper plies. The mirror method uses the inversion of this saddle shape as the mold geometry for the subsequent iteration. However, the reversed saddle shape is much stiffer in bending than the flat plate, which implies that its cure-induced distortions are much lower than the initially flat plate. This leads to a divergence of the compensation method. Besides this robustness issue, the mirror method has the following disadvantages compared to the CAD-based methods developed in [16]:

- the fiber orientations are projected from one mesh to another. They are thus less accurate than with a CAD-centric approach, where a draping simulation is performed for each mold geometry. Moreover, the projection method is valid for small displacements only;
- the compensated shape can take any form which prevents the user from including manufacturing constraints into the design. For instance, it may be necessary for certain regions to remain flat or to follow a fixed curvature;
- since the method is mesh-based, no CAD geometry of the compensated mold is readily available at the end of the procedure. A reverse-engineering step is necessary to reconstruct the geometry, if the mold is to be machined, for instance.

These shortcomings may be improved in the future but they highlight the complementarity of the different methods. The choice of the method depends on the specifications and constraints of the design process. When none of the aforementioned issues are under concern, the mirror method converges much faster towards the optimal compensated shape for the same indicator of distortion D_{min}. Indeed, it does not rely on an optimizer and the number of simulations to be performed is thus drastically reduced.

3. Definition of the validation test case

The C-spar geometry, in Fig. 3, was considered to be an appropriate choice for the experimental study for the following reasons. It is simple enough to be manufactured in Cenaero's research manufacturing lab, yet not too simple avoiding the compensation to be trivial. The dimensions are chosen to be as large as possible, with respect to our manufacturing capabilities, in order to reduce the impact of the process variability and the measurement error. The length of the C-spar is 1225 mm. The parts are processed by Vacuum Assisted Resin Transfer Molding (VARTM). The use of VARTM supposedly leads to poorer quality and higher variability of the produced components compared to industrial processes

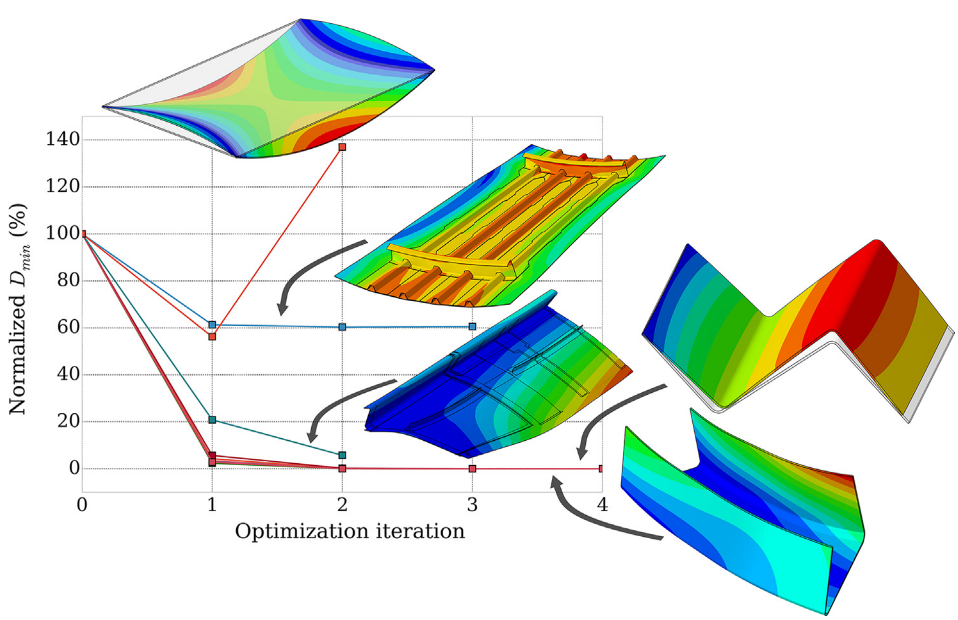

Fig. 2. Convergence history of the mirror method for several geometries.

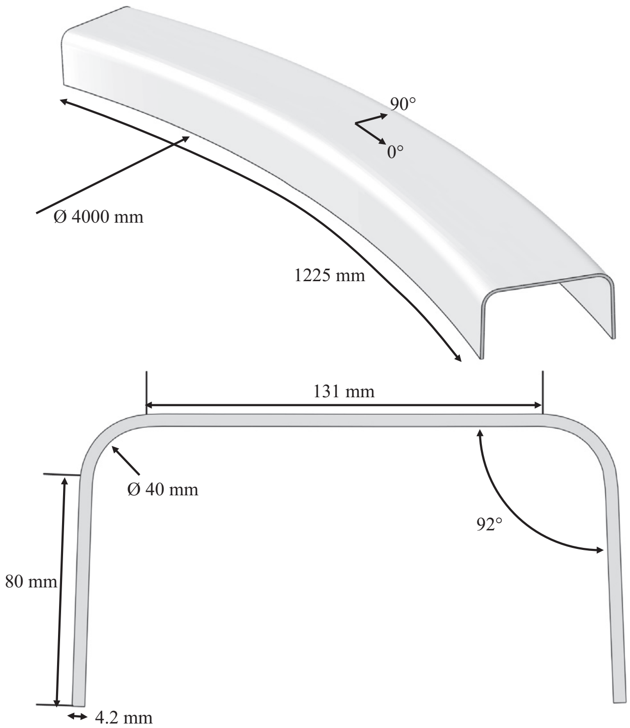

Fig. 3. Nominal geometry of the C-spar for the experimental validation.

such as RTM or autoclave. These issues are mitigated by choosing a rather thick stacking sequence, $[0,45]_{6S}$, resulting in a 12-ply layup which is approximately 4.2 mm thick. Producing thicker parts tends to decrease the variability [17,18]. The selected materials consist of a carbon 5-harness satin weave for the fibers and the aeronautical grade epoxy RTM6 by Hexcel for the matrix. The choice of this resin is driven by the following considerations:

- suitability for vacuum infusion;
- infusion at 80 °C, which makes it easier to control than cheaper resins which are processed at room temperature;
- extensive use in the aeronautics industry, which makes it more interesting to study;
- wide characterization in recent studies [19,20], allowing properties to be extracted and cross-checked from various sources. Most of the RTM6 properties listed in Section 5.2.1lie between values found in other references.

4. Experimental procedure

4.1. VARTM setup

The setup for the infusion process is described in Fig. 4. The one-sided mold is made of aluminum. It is a male mold, which enables easier draping of the carbon plies compared to a female one. Chemlease 1009W release agent is applied over the mold surface four times between each infusion (ten times before the first infusion). Airtac 2 adhesive is lightly sprayed on the top surface of the mold so that the fibers stay in place once they are draped. Next, the carbon plies are carefully laid by hand, starting from the center of the C-spar and progressing in a symmetric manner to the sides. A peel ply is placed on top of the layup in order to ease the removal of the other materials after demolding. Then, a flow medium covers two thirds of the surface. It has a higher permeability than the fibers and thus helps increasing the speed of the infusion by allowing the resin to flow above the fibers and then through the thickness. The flow medium does not cover the entire surface and stops slightly before the vacuum line, so that the resin has time to permeate through the thickness everywhere. An issue with the VARTM process when manufacturing thick composites is that the vacuum bag is likely to pinch the fibers, creating wrinkles in the corner areas which are detrimental to the spring-in behavior [21]. This could be mitigated by a time-consuming step of pre-compaction of the layup by small groups of plies. Here, this step is avoided by adding a silicon sheet on top of the layup. The relatively large thickness of the silicon layer, about 3 mm, makes impossible the pinching of the plies by the vacuum bag. Therefore, the applied pressure is uniform and the corners are smooth. The configuration presents more or less a rotational symmetry and Fig. 4 should be understood as a cross-section view. In particular, the resin inlet and outlet are evenly distributed along the length of the C-spar, with help of spiral tubes. This ensures a regular flow front and reduces the risk of appearance of dry spots. The air tightness of the whole setup is checked by isolating it from the vacuum pump before the infusion, allowing a vacuum drop of less than 1 mbar/min.

4.2. Processing conditions

The infusion follows the manufacturer recommended processing conditions for the RTM6 [22]. The mold is pre-heated to 120 °C for one night. During that time, and after storage at −26 °C, 2 kilograms of RTM6 resin are heated to room temperature. The resin is then poured into a 10-liter injection piston which is

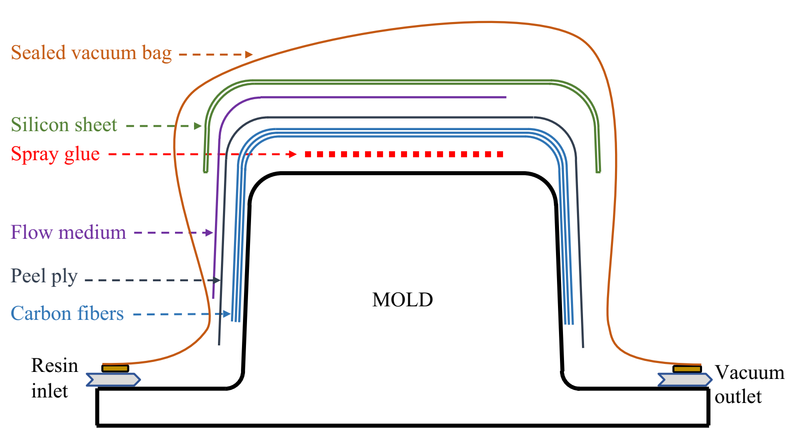

Fig. 4. Setup for the VARTM process.

slowly heated up to 80 °C. Once this temperature is reached, vacuum is switched on and kept for 2 h to remove the air entrapped inside the resin. Next, the infusion is engaged. It takes approximately 15 min for the resin to reach the vacuum outlet. When the infusion is complete, the outlet and inlet are closed and the curing cycle begins. The latter consists of a heating ramp of 1.5 °C/min up to 180 °C, followed by a two-hour dwell. Since the oven has no cooling regulation, its door is simply opened at the end of the dwell. A heat survey showed that this leads to a cooling rate of about 1 °C/min, which is therefore the value that is used in the numerical model.

4.3. Measurements

The mold-facing surface of the manufactured parts is digitized with a Nikon MMDx 100 laser scanner, mounted on a MCA II 7-axis articulated arm of a diameter of 1.8 m. The declared accuracy is 54 μm, although calibration tests show that it is in fact around 30 μm. This leads to a conservative estimation of the measurement error for the spring-in angles of ±0.05°. The obtained point clouds allow tailored post-treatment and measurements of the quantities of interest which are detailed later. The manufactured parts and simulated parts are post-processed with exactly the same technique. The results are provided in Section 6, where they are compared to the results of the process simulation. Fig. 5(a) presents a picture of a manufactured C-spar.

5. Numerical model

5.1. Hypotheses and constitutive model

A simulation-driven compensation methodology requires a numerical model to predict the cure-induced distortions. In summary, the procedure is based on the software Simulayt for the prediction of the fiber orientations and on the FE package Abaqus for the prediction of the distortions, as well as on the following assumptions:

- The temperature is uniform and follows the imposed curing cycle. The choice of imposing a uniform temperature has been made to speed up the simulations but it is not a limitation of the model.
- The infusion step is not modeled. It is thus assumed that the curing process starts when the entire composite part is injected.
- The mold is modeled as a rigid surface to reduce the computational cost of the curing simulations. This is a simplifying assumption since the mold will deform due to thermal expansion, especially with an aluminum mold. This phenomenon can affect the cure-induced distortions. For instance, when injecting and when curing the resin, the mold is larger than at ambient temperature. After cool-down to ambient temperature at the end of the cure cycle, the parts end up being larger than the mold because their coefficient of thermal expansion is generally smaller so that they do not shrink back to the initial size

(a) (b)

Fig. 5. (a) Picture of a manufactured C-spar and (b) typical volume mesh used for the FE prediction of the distortions of the C-spar. The part is meshed with twelve elements through the thickness, i.e. one element per ply.

of the mold. This effect will therefore not be taken into account in the curing simulations and, hence, not be mitigated by the compensation procedure. However, the results presented in the sequel show that the whole procedure already makes it possible to improve significantly the dimensional accuracy of the parts. It can reasonably be assumed that this accuracy could be further improved by including the thermal deformation of the mold in the curing simulations.

- The stick-slip condition developed by Khoun and Hubert [23] is used for the interaction between the part and the mold. For an aluminum mold, this condition implies that the contact is sticking while the shear stress at the interface remains below the threshold τ_{max} = 126 kPa, above which the contact is sliding with a coefficient of friction of 0.3.

In this study, the C-spar is meshed with about 100,000 first-order fully-integrated hexahedra, with one element per ply in the thickness direction, as shown in Fig. 5(b). Typical computational time for the curing simulation is about one hour on six processors of a high performance computing center consisting of Intel E5-2967v2 (2.7 GHz) processors. The constitutive model of the curing thermoset-based composite is implemented through a user subroutine in order to predict the cure-induced distortions. It can be summarized as:

$$\begin{cases} \sigma_{ij} = C_{ijkl}\varepsilon^{el}_{kl} & T \geqslant T_g(X), \\ \dot{\sigma}_{ij} = C_{ijkl}\dot{\varepsilon}^{el}_{kl} & T < T_g(X), \end{cases}$$
$$\varepsilon^{el}_{kl} = \varepsilon_{kl} - \varepsilon^{E}_{kl}, \tag{2}$$
$$\dot{\varepsilon}^{E}_{kl} = \begin{cases} \beta^{r}_{kl}\dot{X} + \alpha^{r}_{kl}\dot{T} & T \geqslant T_g(X), \\ \beta^{g}_{kl}\dot{X} + \alpha^{g}_{kl}\dot{T} & T < T_g(X), \end{cases}$$

where the superscripts r and g denote the rubbery and glassy states, respectively, X is the degree of cure, T is the temperature in degrees Celsius and T_g is the glass transition temperature. σ_{ij} and ε_{kl} are the components of the stress and total strain tensors, respectively; ε^{el}_{kl} are the components of the elastic strain tensor and ε^{E}_{kl} are the components of the misfit strain tensor aggregating the effect of thermal expansion and curing, which is purely dilatational. α and β are the coefficient of thermal expansion (CTE) and coefficient of chemical shrinkage, respectively. Summation over repeated indices is implicit. Eq. (2) is equivalent to the model developed by Svanberg and Holmberg [1] with the following adjustment: here, the elastic tensor C gradually shifts between the rubbery and the glassy states, whereas Svanberg and Holmberg use an abrupt transition. This smooth transition is implemented as follows:

$$C = \begin{cases} C^{r} & T^{*} \geqslant T^{*}_{C}, \\ C^{r} + \frac{T^{*}-T^{*}_{C}}{2T^{*}_{C}} & -T^{*}_{C} < T^{*} < T^{*}_{C}, \text{with} \quad T^{*} = \dfrac{T - T_g(X)}{T_g(X)}. \\ C^{g} & T^{*} \leqslant T^{*}_{C}, \end{cases} \tag{3}$$

Eq. (3) basically implies that the stiffness of the composite is linearly interpolated between that of the rubbery and the glassy states when the temperature T is close to the glass transition temperature T_g. A value of 0.01 for the dimensionless parameter T^{*}_{C} has proved to provide good predictions with respect to experiments [24]. The stiffness tensors of the composite C^{r} and C^{g}, as well as α and β, are determined by homogenization in Section 5.2.3, from the properties of the constituents (resin and fibers).

5.2. Material properties

5.2.1. Properties of the RTM6 epoxy resin

The degree of cure X of the resin is computed during the course of the curing cycle by integrating the cure kinetics model of Karkanas and Partridge [25] for the RTM6:

$$\frac{dX}{dt} = k_1(1-X)^{n} + k_2X^{m}(1-X)^{p}, \tag{4}$$

with $k_i = A_i\exp(-E_i/R(T+273.15))$, $A_1 = 2.6\times10^{4}\mathrm{s}^{-1}$, $A_2 = 5.78\times10^{4}\mathrm{s}^{-1}$, $E_1 = 7.469\times10^{4}\mathrm{J.mol}^{-1}$, $E_2 = 5.837\times10^{4}\mathrm{J.mol}^{-1}$, $m = 1.217$, $n = 0.449$, $p = 1.786$. The glass transition temperature T_g is computed in degrees Celsius with the DiBenedetto equation fitted by Karkanas and Partridge [26]:

$$T_g = -11 + 217\frac{0.435X}{1-0.565X}. \tag{5}$$

The gel point X_{gel} of the RTM6 resin is taken equal to 0.59 [27]. An assumption of the numerical model is that the thermal expansion of the resin does not create stresses nor distortions in the liquid state, i.e. when $X \leq X_{gel}$ [1]. The components of the dilatational strain ε^{E}_{kl} are set to zero below the gel point. The isotropic CTE of the resin is taken from [28]:

$$\alpha = \begin{cases} 136\times10^{-6}\circ C^{-1} & T \geqslant T_g(X), \\ 54\times10^{-6}\circ C^{-1} + 0.16\times10^{-6}\circ C^{-2}T & T < T_g(X). \end{cases} \tag{6}$$

The density difference between the uncured and the cured states is $\Delta V/V$ = –0.046 [28]. Since no information is provided regarding the evolution of the chemical shrinkage during the curing cycle, a constant linear isotropic coefficient of chemical shrinkage $\beta = (\Delta V/V)/3$ = –0.015 is assumed.

In the glassy state, the Poisson's ratio of the resin is considered to be constant and equal to 0.38 [29], and the dependency of the elastic modulus versus the temperature is fitted with data from [19]: $E = -5.93T + 2850$ MPa. In the rubbery state, the resin is assumed to be incompressible [30,31], i.e. the Poisson's ratio ν is equal to 0.5, and the Young's modulus is derived from the procedure proposed by Svanberg et al. [30], which mainly consists in assuming that the shear modulus of the resin is divided by 100 compared to the glassy state. The resulting value for the Young's modulus is E = 29 MPa. An alternative assumption [32] is a ratio equal to 1000 between the Young's modulus in the glassy state and in the rubbery state. This would lead to $E \approx 4$ MPa in the rubbery state. In practice, both values are sufficiently low so that choosing one or the other has no impact on the predicted distortions.

5.2.2. Thermo-elastic properties of the carbon fibers

The carbon textile manufactured by Porcher is a balanced 6k 5-harness satin with a surface density of 375 g/m^2 and 4.6 yarns/cm. Without further information on the type of carbon fibers, these are assumed to have the same properties as T300 fibers [33]: E_L = 230 GPa, E_T = 40 GPa, ν_{LT} = 0.26, G_{LT} = 24 GPa, G_{TT} = 14.3 GPa, α_L = -0.7×10^{-6} °C^{-1}, α_T = 15×10^{-6} °C^{-1}, where the subscripts L and T stand for the longitudinal and transverse directions of the fibers, respectively. This assumption should have only a limited impact on the numerical prediction of cure-induced distortions since these are mainly driven by the properties of the resin in the glassy state [34].

5.2.3. Thermo-elastic properties of the composite

The properties of the composite are determined as follows. Six flat samples of the composite are extracted from the nominal C-spars. The term "nominal" means that the parts are manufactured using a non-compensated mold. The samples are examined by optical microscopy in order to measure the dimensions of the yarns. From 145 measurements, the yarns are determined to be ellipses with major and minor axes equal to 2.18 ± 0.11 mm and 0.204 ± 0.017 mm, respectively. The total fiber volume fraction (FVF) inside the composite is determined by two different techniques, by measuring the thickness and the weight of the samples.

The FVF is equal to 60 ± 2% and the ply thickness is equal to 0.353 ± 0.011 mm. These data are then fed into the FE homogenization framework developed by Wucher et al. [35] to determine the effective thermo-elastic properties of the composite material. The results are provided in Table 1. These properties are then used in the simulations to predict the cure-induced distortions.

The fact that the composite samples are extracted from the nominal C-spars does not make the manufacturing of the nominal parts (and thus the machining of the nominal mold) necessary. These samples can also be simple flat plates, manufactured under the same conditions as the real geometry. The purpose of mold compensation with the help of numerical simulation is indeed to avoid the manufacturing of nominal parts. In the context of this study, it was found appropriate to manufacture nominal parts in order to build confidence in the numerical model, and to execute a complete compensation cycle from both numerical and experimental aspects. This also allows the determination of the gap between the non-compensated geometry, the compensated geometry and the target perfect geometry.

Table 1
Homogenized properties of the satin-epoxy composite. The temperature T is in degrees Celsius. The directions x and y are the in-plane directions of the composite, while the direction z is the through-thickness direction.

Rubbery state		
$E_x = E_y$	[MPa]	23 512
E_z	[MPa]	393
ν_{xy}	[–]	0.54
$\nu_{xz}=\nu_{yz}$	[–]	0.55
G_{xy}	[MPa]	57
$G_{xz} = G_{yz}$	[MPa]	42
$\alpha_x=\alpha_y$	[°C^{-1}]	-1.1×10^{-6}
α_z	[°C^{-1}]	183×10^{-6}
$\beta_x=\beta_y$	[–]	4.2×10^{-5}
β_z	[–]	-1.9×10^{-2}
Glassy state		
$E_x = E_y$	[MPa]	71 964 – 19.2T
E_z	[MPa]	13 451 – 22.3T
ν_{xy}	[–]	0.073
$\nu_{xz}=\nu_{yz}$	[–]	0.459
G_{xy}	[MPa]	4701 – 8.5T
$G_{xz} = G_{yz}$	[MPa]	3287 – 6.1T
$\alpha_x=\alpha_y$	[°C^{-1}]	2.8×10^{-6}
α_z	[°C^{-1}]	$47.1 \times 10^{-6} + 0.12 \times 10^{-6}\ T$
$\beta_x=\beta_y$	[–]	-6.4×10^{-4}
β_z	[–]	-1.1×10^{-2}

6. Results

6.1. Nominal parts

Five nominal C-spars, i.e. based on the geometry of Fig. 3, are manufactured and measured according to the procedure presented in Section 4. The spring-in is computed as illustrated in Fig. 6. Planar sections are extracted perpendicularly to the length of the C-spar. After excluding the round corners, straight lines are fitted to the top and to the sides of each section (bold continuous lines in the sections of Fig. 6). The angles N_i, D_i in the inner curvature, and N_o, D_o in the outer curvature, are measured between these fitted lines. The warpage of the sides is ignored, which is reasonable considering their small dimensions. The nominal angles N_i and N_o are measured on the CAD geometry and the deformed angles D_i and D_o are measured on the digitized manufactured parts. The spring-in is then computed as $S_o=N_o - D_o$ and $S_i=N_i - D_i$. A positive spring-in angle therefore means that the as-manufactured angle D_o or D_i is smaller than its nominal counterpart N_o or N_i. The twist of the part is also quantified by measuring the angle H between the base line and the horizontal plane. It should be pointed out that, since the measurements are performed after a best-fit operation, the angle H is actually an objective measure of the twist. The comparison between the experimental measurements and the simulation is provided in Figs. 7 and 8 for S_i and S_o, respectively. The error bars represent the standard deviations over all the experiments. The simulation underestimates slightly but systematically the spring-in angle by approximately 0.10–0.15° with respect to the averaged experimental results. The experimental variability lies between 0.07° and 0.15°, which is not negligible compared to the absolute value of the spring-in (1° to 1.5°). It is however reasonable considering the use of the VARTM process and the fact that the parts are produced in a lab-scale, non-industrial environment. There is no doubt that a high-pressure process with better quality control (ply cutting and draping, temperature homogeneity, pre-

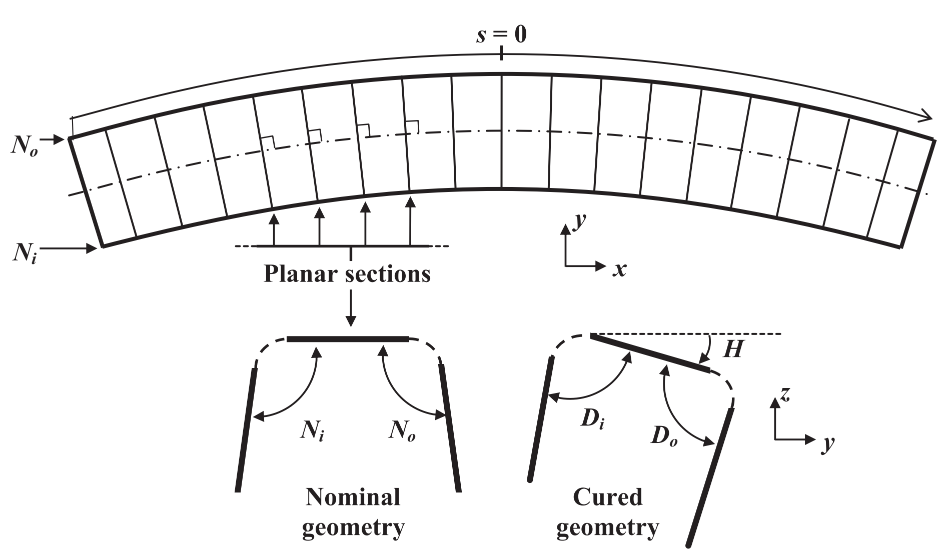

Fig. 6. C-spar spring-in and twist measurement: notations. The spring-in angles are calculated as $S_o = N_o - D_o$ and $S_i = N_i - D_i$.

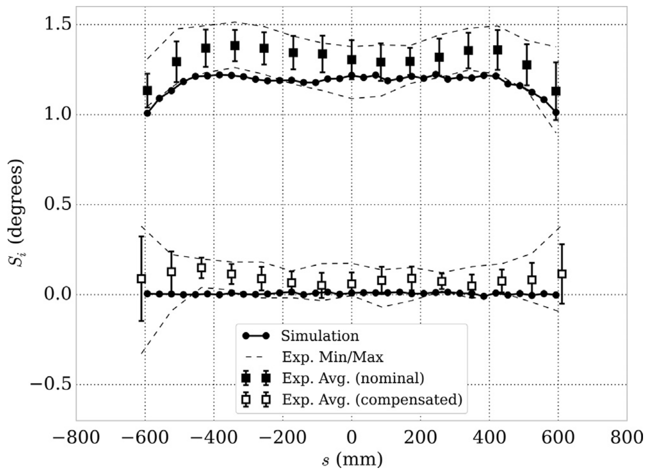

Fig. 7. Comparison between the experiments and the simulations for nominal and compensated parts: internal spring-in S_i.

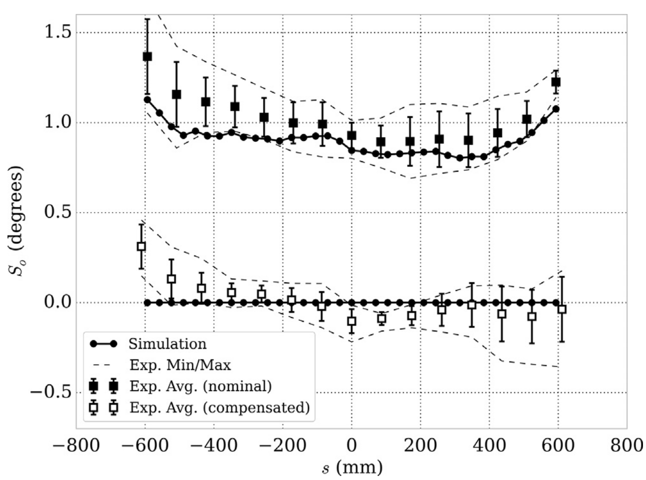

Fig. 8. Comparison between the experiments and the simulations for nominal and compensated parts: external spring-in S_o.

dictable injection path) would result in a much better repeatability. All things considered, the agreement between the experiments and the simulation is satisfactory in terms of the spring-in angle. An important result is that the predicted and measured variations along the length of the spar are similar: the spring-in is more or less constant in the middle of the part, with a decrease (respectively increase) at the free edges for the angle in the inner (respectively outer) curvature.

Regarding the twist H, the comparison is less satisfactory, see Fig. 9. A strong asymmetry, always in the same direction, can be observed for the manufactured parts. This is clear when considering Fig. 10 which presents color maps of the deviations between the manufactured parts and the nominal CAD geometry. A positive deviation means that the experiment is "above" the CAD geometry. Fig. 9 includes least-square fitted parabola for all the experiments which shows that the twist can be accurately represented by a parabola. The asymmetry may come from different sources of deviation from the "ideal" situation: tolerances in the machining of the mold, deviations in the fiber orientations, non-uniformity of the infusion or of the curing process, to name a few. Since the analysis of the manufacturing of the compensated parts in Section 6.2 brings additional information, these potential causes are discussed later in the paper.

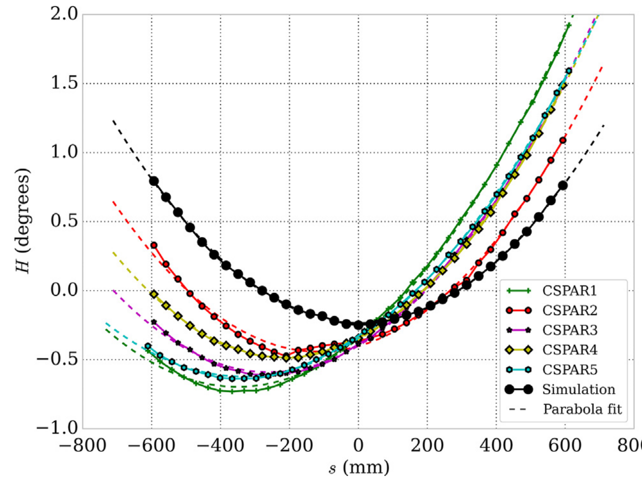

Fig. 9. Comparison between the experiments and the simulations for the twist (nominal parts).

To conclude, even though the manufacturing of the nominal parts was not necessary to proceed to the compensation step, the results show the level of confidence that can be put in the model, before looking at the question of the compensation itself. It quantifies the first source of error which is independent of the compensation strategy. It is clear that the spring-in is much better predicted than the other main distortion mode, i.e. the twist. If the imperfection of the manufacturing process is not related to the mold itself, and if it is not identified and solved, there is a high probability that the twist will not be properly compensated. It should be pointed out that the twist is probably a less detrimental distortion than spring-in. Indeed, correcting the twist most likely requires less effort during the assembling step than correcting for spring-in.

6.2. Compensated parts

A compensated mold geometry is generated by applying the numerical compensation procedure. The distortions measured on the manufactured nominal parts are not used in this process, for which the only required experimental data are related to the geometry of the textile, as discussed in Section 5.2.3. The mold is machined at Cenaero with a CMS Antares 5-axis numerically-controlled milling machine and finished off with sandpaper to obtain a smooth surface finish. Five C-spars are manufactured and measured under the same conditions as previously described in Section 4. The measured spring-in angles are reported in Figs. 7 and 8, where they can be compared to the spring-in of the nominal parts. The spring-in has been reduced to less than 0.1°, on average, again with some variability. The spring-in is less than 10% of the original spring-in of the non-compensated spars, which is a very satisfactory achievement.

The twist measurements for all the compensated parts are shown in Fig. 11. Once again there is a clear asymmetry. While the measured twist of the compensated parts should be zero, it is instead linear. This is very interesting when considering the observation made for the nominal parts. Indeed, the twist of the nominal parts could be approximated by a quadratic polynomial. The numerical simulation captures well the second order coefficient: the value of this coefficient varies experimentally between 86% and 106% of the value of the simulation, with an average within 1% of the one predicted by the simulation. However, the linear part of the polynomial fit is not well predicted: the parabola of the nominal experiments is shifted with respect to the predictions.

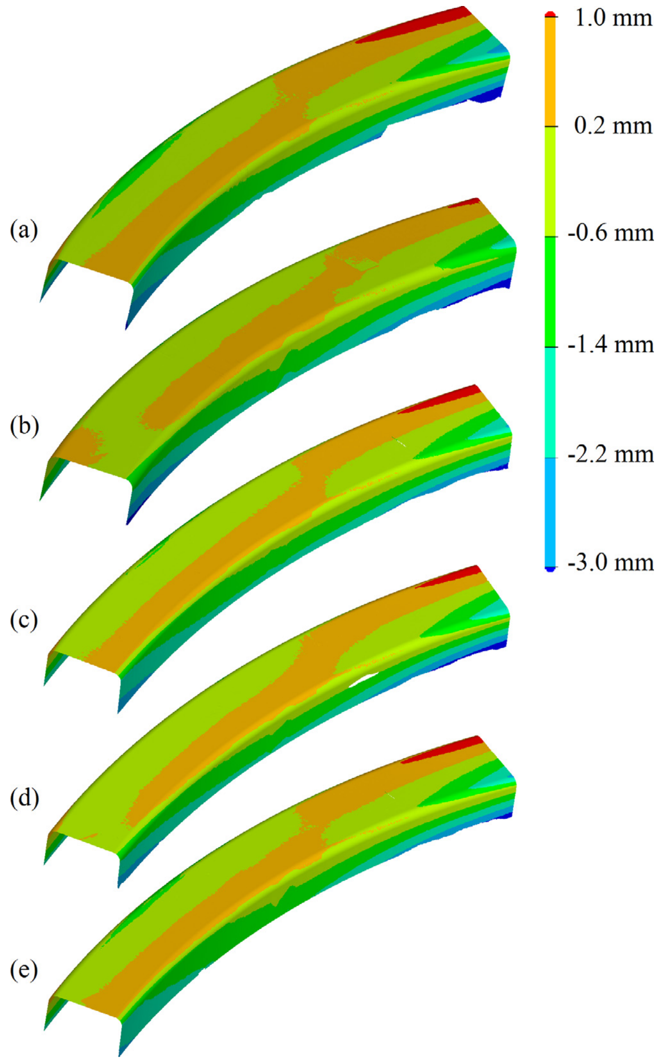

Fig. 10. Deviations between the manufactured nominal parts and the nominal CAD model.

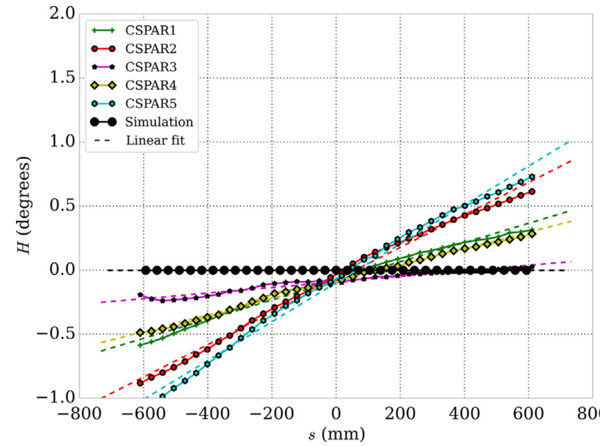

Fig. 11. Comparison between the experiments and the simulations for the twist (compensated parts).

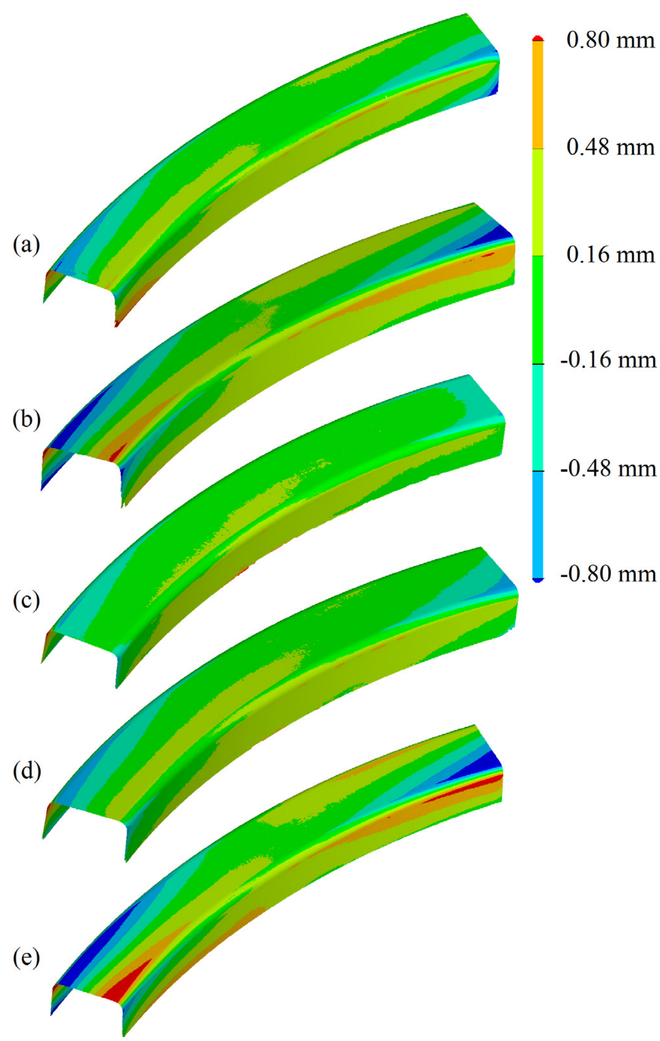

Fig. 12. Deviations between the manufactured compensated parts and the nominal CAD model.

Therefore, it can be speculated that the twist of the nominal manufactured parts is a quadratic polynomial, plus a linear function due to an unpredicted asymmetry in the manufacturing process. Since the latter is not taken into account in the simulation, the compensation procedure has suppressed the quadratic part of the twist only. Following this rationale, it makes sense that the twist of the compensated parts should be linear. Although this is only a conjecture, it is strongly supported by the analysis of Figs. 9 and 11.

The distortions of the compensated parts can also be analyzed in terms of the statistics of the overall deviations. As for nominal parts, color maps are created to represent the deviation with respect to the nominal geometry, see Fig. 12. The color scale is adapted for better visualization: the scale ranges from -0.8 mm to 0.8 mm for the compensated parts in Fig. 12, while it ranges from -3 mm to 1 mm for the nominal parts in Fig. 10. Each color map is made of a point cloud of about 500,000 points, which constitute thus a suitable basis to study the deviations from a statistical point of view. Firstly, Fig. 13 shows the dispersion of the deviations, in the form of histograms, for both the compensated and nominal configurations. The dispersion is much lower for the compensated parts, and the distribution of the deviations is much more condensed around zero, which is the target of the compensation. The bottom graph, marked "ALL", considers the point clouds of all the parts combined. Secondly, Table 2 presents percentiles of the cumulative distributions of the absolute deviations. The percentiles give the number of points which are below a certain

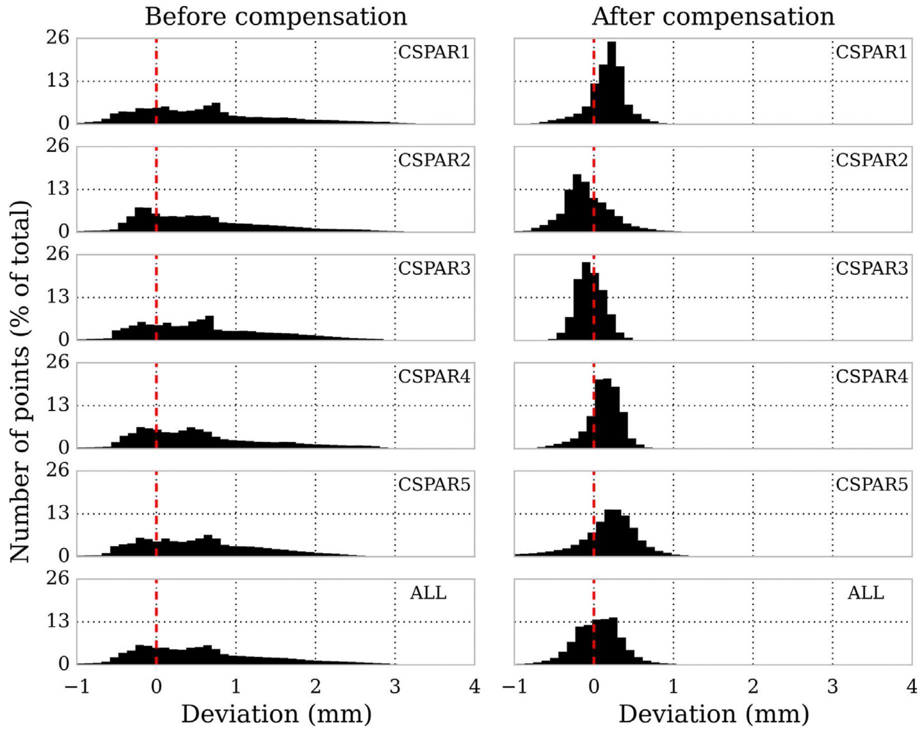

Fig. 13. Histograms of the deviations between the manufactured parts and the nominal CAD model.

Table 2
Absolute deviations between the manufactured parts and the nominal geometry.

Percentile	Nominal parts (mm)	Compensated parts (mm)	Relative difference
5-th	0.051	0.018	−65%
10-th	0.102	0.038	−63%
25-th	0.253	0.097	−62%
50-th	0.534	0.197	−63%
75-th	1.098	0.325	−70%
90-th	1.813	0.491	−73%
95-th	2.240	0.633	−72%
99-th	2.810	0.951	−66%

threshold. They are calculated based on the combined point clouds, i.e. considering the 5 parts together. The absolute deviations are considered since it does not make sense to compute the percentiles of the signed deviations. For instance, for the compensated parts, 75% of the points deviate by less than 0.33 mm, and 98% by less than 0.81 mm. These numbers go up to 1.1 mm and 2.6 mm, respectively, for the nominal parts. The percentiles of the compensated parts are improved by 62%–73 % in comparison to the nominal parts. This is a good achievement, considering that the twist has not been entirely compensated.

6.3. Origin of the twist

The reasons for the non-compensation of the twist are further discussed in this section. The possible sources of imperfection in the manufacturing process are listed hereafter, among which those that could lead to a repeatable (at least qualitatively) asymmetry are identified:

- *Non-uniform cure due to the infusion process.* The infusion is not simulated numerically and the curing model therefore assumes that the part is fully infused and then starts to cure with an initial degree of cure X equal to zero. This hypothesis misses two different ingredients of the real process. The first one is that the infusion is not instantaneous and the second one is that the flow front may not be perfectly straight. In practice, the regularity of the flow front could not be checked because of the high temperature and because the silicon sheets under the vacuum bag obstruct the view. However, the infusion time has been measured: it takes about 15 min for the resin to travel through the layup before the part is fully infused, after which the real curing cycle is started. During these 15 min, the resin which is infused is heated to 120 °C by the mold and by the surrounding air, while the resin which is not infused yet is still at 80 °C. It can be estimated with the kinetics model, Eq. (4), that the difference of initial degree of cure between any two points of the structure is less than 1%. This is certainly not sufficient to generate the discrepancy which has been observed in the twist behavior between the experiments and the simulation.
- *Non-uniform cure due to a heterogeneous temperature distribution inside the oven.* If there exists a temperature gradient between the left side and the right side of the mold, and if the mold is always placed in the same position in the oven (which is the case), this could explain the asymmetry. A heat survey, executed twice in the same conditions, showed that there is indeed a temperature gradient. During the curing cycle, the left side of the mold is warmer than the right side by 1–3 °C, and warmer than the middle of the mold by 3–8 °C. However, a simulation carried out with these data exhibited no significant effect on the twist.
- *Fiber orientations.* One of the most approximate experimental manipulations, in our context, is the cutting and the draping of the carbon plies, in particular the 45-° plies. The latter easily shear and one must be careful when laying them onto the mold. Although this is clearly a weak point in our manufacturing chain, it is probably not the cause of the asymmetry, and this for two reasons: firstly, it is more a source of variability than

of asymmetry; and, secondly, a simulation where all ply orientations are shifted by 5° demonstrated, once again, no significant effect on the twist.
- *Layup asymmetry*. The layup, made of 5-harness satin, is not perfectly orthotropic and this characteristic may be an additional source of asymmetry. In particular, the top six plies were not turned over with respect to the bottom plies. This effect has not been investigated further.
- *Measurement method*. The parts are laid flat on a table in order to be scanned. Even though they are not mechanically clamped, since this would influence their shape, gravity could also cause this problem. However, considering the stiffness of the C-spar and its weight, this effect is most likely negligible. Moreover, if it does lead to asymmetry, there is no reason why it would always be in the same direction. One could also point out that the best-fit operation between the scanned part and the nominal CAD geometry may influence the value of the twist, which is measured relatively to the horizontal plane. This cannot be the reason for the asymmetry since performing a best-fit between a symmetric scan and a symmetric CAD should maintain the symmetry. If the best-fit was somewhat uncertain, the asymmetry would not be repeatable.
- *Machining accuracy*. The machining process may produce imperfect molds, which could lead to imperfect part production. The deviation between the machined molds and the theoretical CAD shapes has been assessed. No clear asymmetry has been measured for either mold and, more importantly, it is very unlikely that two completely independent molds would suffer from the same defect and produce the same trend of twist imperfection (increasing twist from left to right, see Figs. 9 and 11).

Consequently, a definitive answer on the origin of the observed twist cannot be provided, at this point, as to why all manufactured parts present the same kind of asymmetry. It is possible that some of the assumptions of the numerical simulations hide the real effect of the imperfections listed above. In particular, a slight fiber misalignment could become more significant with the expansion of the mold, which is ignored in the simulations. The potential effect of this assumption on the accuracy of the numerical predictions is left for further studies, since the present paper focuses on the experimental aspects. At this stage, the assumptions of non-uniform cure and fiber misalignment are the most reasonable ones. A very interesting topic of investigation with practical impact would be to study the influence of these imperfections and of the variability on the reject rate in an actual industrial production line.

7. Conclusion

In this study, a computational compensation chain has been developed to produce C-spars with reduced distortions. Besides the geometry, only the properties of the constituents (resin and fibers) and micrographs of the textile have been needed as inputs of the simulation to complete the objective. These micrographs have been extracted from the nominal C-spars, but they could also have been obtained by manufacturing simple flat plates, thus suppressing the need to machine the nominal mold. A good agreement between the simulation of the curing process and the experiments has been demonstrated for two types of geometry (nominal and compensated). While the spring-in effect is qualitatively and quantitatively predicted, which results in a compensation of about 90%, the twist distortion mode is affected by a probable imperfection in the manufacturing process which has not been identified at this stage. The 95-th percentile of the deviations has been reduced from 2.24 mm to 0.63 mm, which makes the compensated parts much more compatible to a subsequent assembly step. Interestingly, the twist has evolved from a parabola to a linear distribution, while, in fact, the second-order coefficient of the parabola has been well-captured by the simulation. This gives the impression that, if the imperfection is identified and accounted for in the simulation, the twist will be properly compensated. The residual twist must therefore be attributed to the manufacturing process and not to the compensation methodology.

The experimental campaign highlights the benefits of using numerical compensation. Direct prediction of the compensated shape spares the cost and time of machining a nominal mold and avoids the need to guess the compensation based on preliminary simulations. Relying on rule of thumbs, e.g. by opening the angle by 1° to compensate for the spring-in, would miss the fact that the spring-in is not constant, and the twist would be simply disregarded.

Acknowledgments

The authors are grateful to Mr A. Hajdu (Cenaero) for machining the compensated mold. This work has been financially supported by the Walloon Region (Belgium) through the First DoCA OPTI-MOLD project (grant number ECV320600FD012F/1117310), and by the European Commission through the ERDF project CILAB (grant number ECV12020022191F).

References

[1] Svanberg JM, Holmberg JA. Prediction of shape distortions Part I. FE-implementation of a path dependent constitutive model. Compos Part A-Appl S 2004;35(6):711–21.
[2] Kappel E, Stefaniak D, Hühne C. Semi-analytical spring-in analysis to counteract CFRP manufacturing deformations by tool compensation. In: Proceedings of ICAS-2012 Conference. Brisbane, September 2012.
[3] Teoh KJ, Hsiao KT. Improved dimensional infidelity of curve-shaped VARTM composite laminates using a multi-stage curing technique – Experiments and modeling. Compos Part A-Appl S 2011;42(7):762–71.
[4] Hsiao KT, Gangireddy S. Investigation on the spring-in phenomenon of carbon nanofiber-glass fiber/polyester composites manufactured with vacuum assisted resin transfer molding. Compos Part A-Appl S 2008;39(5):834–42.
[5] Jain LK, Hou M, Ye L, Mai YW. Spring-in study of the aileron rib manufactured from advanced thermoplastic composite. Compos Part A-Appl S 1998;29 (8):973–9.
[6] Brauner C. Analysis of process-induced distortions and residual stresses of composite structures PhD thesis. Universität Bremen; 2014.
[7] Dong C. Dimension variation prediction and control for composites PhD thesis. The Florida State University; 2003.
[8] Dong C. Process-induced deformation of composite T-stiffener structures. Compos Struct 2010;92(7):1614–9.
[9] Zhu Q, Geubelle PH. Dimensional accuracy of thermoset composites: shape optimization. J Compos Mater 2002;36(6):647–72.
[10] Kappel E, Stefaniak D, Spröwitz T, Hühne C. A semi-analytical simulation strategy and its application to warpage of autoclave-processed CFRP parts. Compos Part A-Appl S 2011;42(12):1985–94.
[11] Jung WK, Chu WS, Ahn SH, Won MS. Measurement and compensation of spring-back of a hybrid composite beam. J Compos Mater 2007;41(7):851–64.
[12] Fernlund G, Osooly A, Poursartip A, Vaziri R, Courdji R, Nelson K, et al. Finite element based prediction of process-induced deformation of autoclaved composite structures using 2D process analysis and 3D structural analysis. Compos Struct 2003;62(2):223–34.
[13] Fernlund G, Floyd A. Process analysis and tool compensation for curved composite L-angles. In: Proceedings of CANCOM-2007 Conference. Winnipeg, August 2007.
[14] Fernlund G. Risk reduction in composites processing using prototype data, process simulation, and Bayesian statistics. Compos Part A-Appl S 2010;41 (2):295–303.
[15] Hörberg E, Nyman T, Hellström T, Rudlund M, Bohlin J, Berg R. Shape distortion analysis of a complex shaped wing skin section. In: Proceedings of ICCM-20 Conference. Copenhagen, July 2015.
[16] Wucher B, Lani F, Pardoen T, Bailly C, Martiny P. Tooling geometry optimization for compensation of cure-induced distortions of a curved carbon/epoxy C-spar. Compos Part A-Appl S 2014;56:27–35.
[17] Parmentier A, Wucher B, Martiny P. Experimental and numerical study of the cure-induced deformations in composites produced by vacuum infusion. In: Proceedings of ICCM-19 Conference. Montreal, July 2013.
[18] Albert C, Fernlund G. Spring-in and warpage of angled composite laminates. Compos Sci Technol 2002;62(14):1895–912.
[19] Morelle XP, Chevalier J, Bailly C, Pardoen T, Lani F. Mechanical characterization and modeling of the deformation and failure of the highly crosslinked RTM6

epoxy resin. Mech Time-Depend Mater 2017. http://dx.doi.org/10.1007/s11043-016-9336-6.
[20] Chevalier J, Morelle XP, Bailly C, Camanho PP, Pardoen T, Lani F. Micro-mechanics based pressure dependent failure model for highly cross-linked epoxy resins. Eng Fract Mech 2016;158:1–12.
[21] Potter K, Khan B, Wisnom M, Bell T, Stevens J. Variability, fibre waviness and misalignment in the determination of the properties of composite materials and structures. Compos Part A-Appl S 2008;39(9):1343–54.
[22] Hexcel. Hexflow®RTM6. Product datasheet, December 2014.
[23] Khoun L, Hubert P. Cure shrinkage characterization of an epoxy resin system by two in situ measurement methods. Polym Compos 2010;31(9):1603–10.
[24] Parmentier A, Wucher B, Dumas D. Determination of the model complexity level required to predict the cure-induced deformations in thermoset-based composite parts. In: Proceedings of ECCM-16 Conference. Sevilla, June 2014.
[25] Karkanas PI, Partridge IK. Cure modeling and monitoring of epoxy/amine resin systems. I. Cure kinetics modeling. J Appl Polym Sci 2000;77(7):1419–31.
[26] Karkanas PI, Partridge IK. Cure modeling and monitoring of epoxy/amine resin systems. II. Network formation and chemoviscosity modeling. J Appl Polym Sci 2000;77(10):2178–88.
[27] Karkanas PI. Cure modelling and monitoring of epoxy/amine resin systems PhD thesis. Cranfield University; 1998.
[28] Skordos AA, Partridge IK. Monitoring and heat transfer modelling of the cure of thermoset composites processed by resin transfer moulding. In: Proceedings of the International Symposium on Polymer Composites Science and Technology. Québec, October 1999.
[29] Hobbiebrunken T, Fiedler B, Hojo M, Ochiai S, Schulte K. Microscopic yielding of CF/epoxy composites and the effect on the formation of thermal residual stresses. Compos Sci Technol 2005;65(10):1626–35.
[30] Svanberg JM, Altkvist C, Nyman T. Prediction of shape distortions for a curved composite C-spar. J Reinf Plast Comp 2005;24(3):323–39.
[31] Ersoy N, Garstka T, Potter K, Wisnom MR, Porter D, Clegg M, et al. Development of the properties of a carbon fibre reinforced thermosetting composite through cure. Compos Part A-Appl S 2010;41(3):401–9.
[32] Johnston AA. An integrated model of the development of process-induced deformation in autoclave processing of composite structures PhD thesis. The University of British Columbia; 1997.
[33] Naik NK, Ganesh VK. An analytical method for plain weave fabric composites. Composites 1995;26(4):281–9.
[34] Parmentier A, Wucher B, Dumas D. Influence of the thermo-mechanical properties on the predictions of the cure-induced deformations in thermoset-based composite parts. In: Proceedings of ICCM-20 Conference. Copenhagen, July 2015.
[35] Wucher B, Hallström S, Dumas D, Pardoen T, Bailly C, Martiny P, et al. Nonconformal mesh-based finite element strategy for 3D textile composites. J Compos Mater 2017;51(16):2315–30.